A Cryogenic Test Rig for Dynamically Operated Plate-Fin Heat Exchangers

Philipp Fritsch[1],*, Rainer Hoffmann[2], Rainer Flüggen[2], Patrick Haider[1], Sebastian Rehfeldt[1], and Harald Klein[1]

Flexible operation of air separation units may lead to enhanced thermal stress on the main heat exchanger, typically an aluminum plate-fin heat exchanger. Hence, a large, cryogenic test rig has been built to investigate fatigue effects of dynamic operation. Nitrogen streams at –175 °C and 50 °C are applied to induce a highly repetitive series of temperature changes in two plate-fin heat exchangers, which are extensively equipped with measurement technology to collect 3D temperature and strain data and to detect the provoked fatigue damages. Results of the measurements will be used to improve computational lifetime estimation tools.

1 Introduction

Four "Kopernikus" projects were introduced by the German Federal Ministry of Education and Research to bundle research concerning the energy transition, i.e., the transfer of power supply away from nuclear and fossil sources towards renewable energies [1]. "SynErgie" is one of these projects, and it aims to increase the flexibility of energy-intensive industrial processes as a means of facing the resulting volatility of energy availability and prices [2]. Air separation is one promising process for stabilizing the power grid, due to the high energy demand of air separation units (ASUs), their widespread application and high-density storage capacity using cryogenic liquid products. Therefore, the subproject "FlexASU" intends to enable such plants to operate in a flexible manner, where partial-load operation or complete shutdown are applied in times of low availability of power from renewable energies [3]. Until now, ASUs, like many large-scale processes, have been designed for steady-state operation at the optimum operating point. Due to the high degree of process integration and highly non-linear behavior [4], shifting towards a load flexible operation is challenging in terms of process control as well as equipment design.

The main heat exchanger, typically an aluminum plate-fin heat exchanger (PFHE), has been identified as one of the critical key components when it comes to lifetime of a flexibly operated ASU [5]. While the number of load changes, startup and shutdown events during the lifetime of an ASU is comparably low (approx. 100) for steady-state operation and mostly limited to maintenance and service shutdowns, this number increases significantly (up to 1000–10 000) if

the ASU is operated flexibly. Load changes may lead to additional thermal stress on the main heat exchanger and eventually cause fatigue damage if the number of events is too high [6, 7].

If a flexibly operated ASU is built, the lifetime of a PFHE must be guaranteed over a certain number of events. This is why a method of assessing the thermal stress caused by transient operating conditions has been developed [8]. The method consists of a thermo-fluid dynamic simulation and a subsequent finite elements analysis, and is described in [6, 9–11] in more detail. The method has already been validated against heat exchangers in the field [6] and experimental thermal fatigue tests using comparatively small PFHEs [12]. However, damage symptoms for these small PFHEs differ from fatigue damages experienced in commercial plants [13]. Hence, validation data from larger, more realistic PFHEs is strongly desired. Approaches for quasi-three-dimensional modeling of steady-state PFHEs are present in the literature (e.g., [14–16]). Usually, fluid redirection by distributors or collectors is not considered in these studies. In the "FlexASU" project, a transient three-

—

[1]Philipp Fritsch, Patrick Haider, Dr. Sebastian Rehfeldt, Prof. Dr. Harald Klein
philipp.fritsch@tum.de
Technical University of Munich, Department of Mechanical Engineering, Institute of Plant and Process Technology, Boltzmannstraße 15, 85748 Garching, Germany.
[2]Dr. Rainer Hoffmann, Rainer Flüggen
Linde GmbH, Linde Engineering, Dr.-Carl-von-Linde-Straße 6–14, 82049 Pullach, Germany.

dimensional model for complete PFHEs including these effects has been developed [11], which can be used in lifetime estimation. The model has already been validated against literature data and simulation results from commercial software [11]. Experimental three-dimensional temperature data is required for further validation of the model. Unfortunately, heat exchangers in commercial plants are not suitable for collecting this data. In steady-state operation, which is the predominant operation mode up to now, only few data from highly dynamic operation is accessible and damage events are very rare. Additionally, commercial PFHEs are not equipped with the necessary measurement devices. In most cases, heat exchangers (HEX) in the field are solely equipped with the metrology that is prerequisite for process control.

For this reason, a large test rig was built to collect all required data for validating the new three-dimensional thermo-fluid model [11] and improved computational lifetime estimation tools. In the test rig nitrogen at –175 °C and 50 °C is applied to induce a highly repetitive series of temperature changes in two plate-fin heat exchangers. The test rig should be capable of recording 3D temperature and strain data in transient operation conditions and detecting time and location of the appearance of a provoked fatigue damage, which is why it is extensively equipped with measurement technology. The design of the test rig is described in [10]. Now, since the test rig has been built and put into operation, this paper will provide additional information about structure and operation of the test rig and, in particular, describe the installed, partially advanced measurement systems including some exemplary results.

2 Main Heat Exchangers in Air Separation Units

The predominant method of separating air into its main components oxygen and nitrogen is by cryogenic distillation. In this process, ambient air is filtered and compressed in the main air compressor. After passing a precooling and an adsorber station, where interfering components (e.g., water, CO_2) are removed, the feed enters the cryogenic part of the ASU, which is enclosed by a perlite-filled coldbox. Within the main heat exchanger, the air stream is cooled against cold ASU products. Hence, the main heat exchanger acts as a thermal link between ambience and the cryogenic ASU process. Afterwards the actual separation of the components is achieved in a pressure-staged double column. Using additional columns, argon may also be obtained from the air stream. More detailed information about cryogenic separation of air can be found in [4, 10, 17–19].

Main heat exchangers in air separation units are almost exclusively aluminum plate-fin heat

exchangers [20]. This kind of heat exchanger combines a high level of process integration, containing up to 12 process streams [20], and a compact design due to the high surface area. Aluminum heat exchangers can be used for pressures up to 130 bar and temperatures between –269 °C and 93 °C [21], which covers the operating range of an ASU. Each PFHE consists of a sequence of layers, which are brazed together to form a block [22]. Each layer is formed by parting sheets and side bars, between which a fin structure is installed to obtain a high surface area for heat transfer (see Fig. 1a). Furthermore, PFHEs consist of distributing and collecting fins, headers and nozzles, which either collect or distribute the process streams over the layers (see Fig. 1b).

Due to the manufacturing process, there are certain limitations on the maximum spatial dimensions of a PFHE block. If a larger heat transfer area is required, several PFHE modules are welded together [13].

3 Experimental Setup

This section describes the test scenario, the PFHE specimen installed and the overall test rig, before the measurement technology is addressed in a separate section.

3.1 Test Scenario

ASU load changes, shutdowns and startups cause the main heat exchanger to cool down and warm up. Therefore, the PFHEs are repeatedly heated and cooled in the test rig in a test scenario to investigate transient conditions and thermal fatigue of the equipment. Several requirements must be fulfilled in order to achieve reasonable test rig operation. The results shall be representative for large-scale PFHEs in the field. Consequently, the test rig is operated with gaseous nitrogen as a process medium. Temperature and pressure levels in the test rig are chosen in a similar manner to commercial ASUs. The test scenario is deliberately designed to be faster and more harmful than commercial plant load changes to achieve a fatigue damage in a foreseeable period
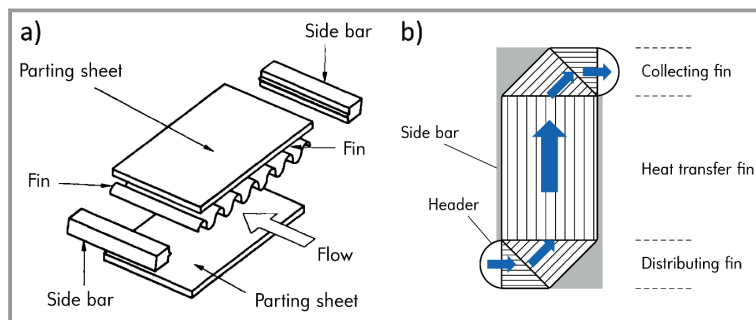

Figure 1. a) Components of a PFHE layer (adapted from [20]) and b) exemplary stream pathway through a PFHE layer.

of time. In contrast to commercial plants, in which different load changes do occur, repeatable temperature changes are desired in the test scenario and numerically challenging conditions, such as phase changes, are avoided to simplify reproducing the test scenario using the thermo-fluid model and subsequent finite element analysis. Further considerations that led to this test scenario can be found in [10].

The sequence of one cooldown and one warmup phase is defined as one cycle. At the beginning of a cycle, a temperature of approx. 50 °C prevails throughout the PFHE. Then, a mass flow rate of approx. 1000 kg h⁻¹ of gaseous nitrogen at –175 °C is fed to the PFHE. Due to the high temperature difference, the PFHE is subject to high thermal stress, especially right after the cold gas flow is fed to the PFHE. Cooling is continued for around 500 s. This duration is deliberately not long enough for the heat exchanger to cool down completely. As a result, the gas stream leaves the PFHE at a temperature of approx. 50 °C throughout the cycle.

In the next step, the cold gas flow is stopped and the PFHE is warmed up again. For this purpose, a warm gas flow of gaseous nitrogen at 50 °C is directed to the PFHE from the opposite side. Because the temperature difference is smaller now, a larger mass flow rate of nitrogen of approx. 10 000 kg h⁻¹ is required to warm the heat exchanger up in the same duration as the cooldown phase. This large mass flow rate leads to a fast temperature change at the cold end of the PFHE and hence to another peak in thermal stress right after the start of the warm gas flow. After the warmup phase is finished the gas flow is stopped, and the next cooldown phase starts.

This cyclic temperature change operation is carried out fully automatically by the sequencer of a distributed control system (DCS). In contrast to the commercial operation of a heat exchanger, there is no countercurrent flow of the cold and warm gas stream in the test PFHE at any time.

3.2 PFHE Test Specimen

The design of the PFHE specimen for application in the test rig is limited by several constraints. The PFHE shall be large enough to capture all expected effects, but small enough for the complete test rig to fit into the laboratory building and be operated in an economically feasible manner. Furthermore, the test PFHE should consist of at least two modules and contain all areas that were identified as at particular risk of fatigue damage [13]. As a trade-off, two aluminum PFHEs with the following characteristics were manufactured.

The specimens show dimensions of approx. 1.5 m length, 1.5 m height and 0.5 m width, which results in a mass of around 1500 kg and an effective heat exchange area of about 850 m² each. The specimens contain all design elements of a commercial ASU PFHE such as headers, nozzles and fin-containing layers formed by parting sheets and side bars. Fins were chosen to be similar to commercial PFHEs and to

manage the pressure drops of the vastly differing cold and warm mass flow rates (cf. [10]). Each PFHE consists of two modules and is designed for two process streams, which are distributed over around 200 active layers. Additional protection dummy layers and blank layers for measurement instrumentation are provided.

3.3 Test Rig

To subject the PFHEs to the desired test scenario in an efficient closed circular flow operation, a configuration with two parallel PFHEs is chosen. A simplified process flow diagram (PFD) of the test rig is shown in Fig. 2. The warm gas stream is supplied to one PFHE by an electrical heater and a rotary blower. After leaving the PFHE, a small part of the stream is separated and used as cold gas stream for the other PFHE. The stream is cooled by a "Block-in-Kettle" (BiK) cooler using evaporating liquid nitrogen as coolant. After half of the cycle duration, the streams are switched and the PFHEs undergo the opposite temperature program. Since the cooldown and the warmup phases have the same duration, continuously alternating cooldown and warmup phases can be achieved for both PFHEs in total. During operation, a closed circular flow rate of 10 000 kg h⁻¹ gaseous nitrogen prevails in the test rig, and approx. 400 kg h⁻¹ of liquid nitrogen (LIN) is evaporated. In the state shown in Fig. 2, the PFHE A is in cooldown and PFHE B in the warm-up phase. A black filled symbol indicates a closed valve.
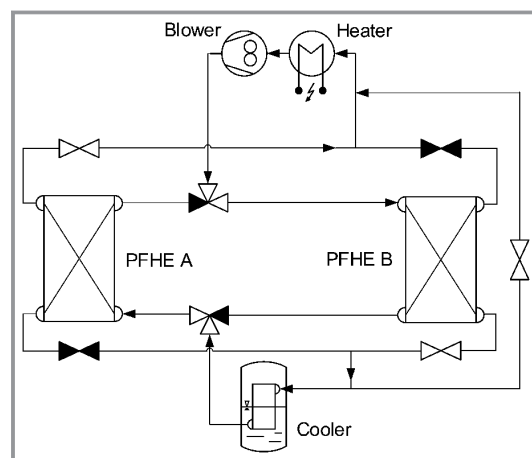

Figure 2. Simplified PFD of the test rig [10].

Due to the cryogenic temperatures, the cold part of the test rig is installed in a coldbox. Perlite is used as isolation material in the coldbox. Contrary to commercial ASUs, the coldbox is not filled to the top with perlite. The warm ends of the PFHEs protrude from the perlite to provide easy access to the installed measurement technology. Another difference from commercial ASUs is that the coldbox is not air-tight and flushed with air instead of nitrogen. This is

possible because process temperatures do not fall below the dew point of oxygen at ambient pressure.

In Fig. 3, a 3D model of the test rig is shown. It is apparent that some auxiliary equipment is required in addition to the basic components shown in the simplified PFD (Fig. 2). The instrument panel is used to supply and withdraw nitrogen from the test rig and carry out leakage tests. The equalizer is used as a thermal mass to ensure a temporally constant temperature in the closed circular flow. The mobile LIN tank supplies the BiK with liquid nitrogen. The drain pit is used for rapid removal of LIN from the BiK. The tank and the drain pit are located outside of the building. The blower and the heater are installed in the basement.

4 Measurement Technology

Several different, partially advanced measurement technologies are installed at the test rig. The devices can be divided in measurement technology used for process control, scientific temperature and strain measurement as well as damage detection.

4.1 Process Control

Like in commercial plants, conventional temperature, flow and pressure sensors are applied for process control. These devices are available in the process control system to monitor and control the operation of the test rig. The location of the sensors is depicted in Fig. 4. As a characteristic feature of the test rig, three Pt100 temperature sensors are attached to the surface of each heat exchanger at different heights to
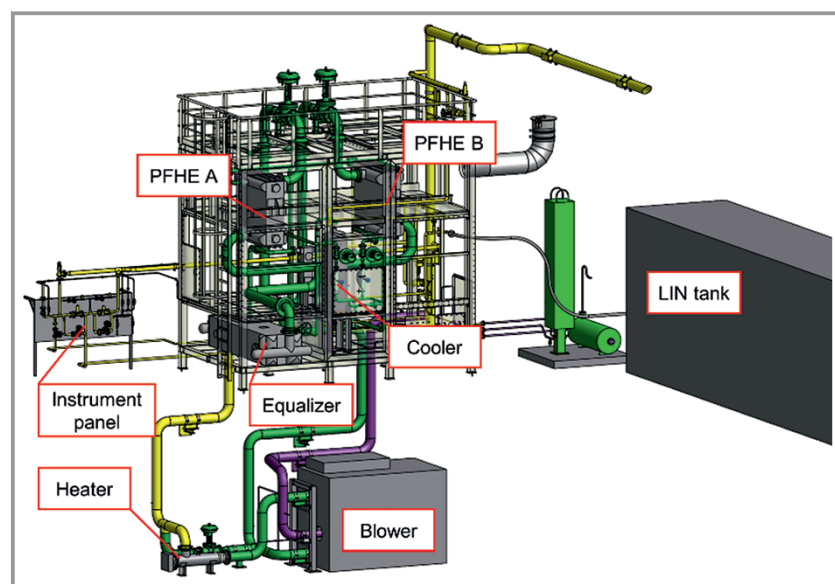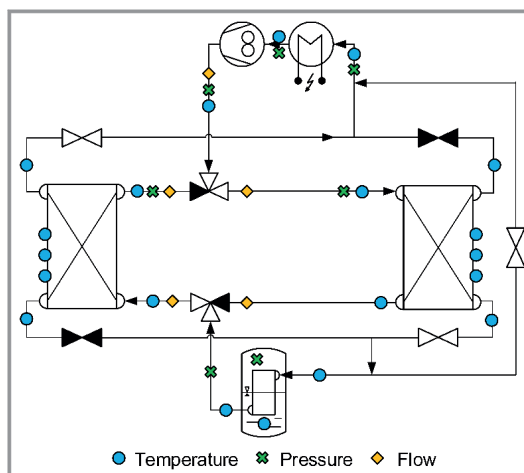
Figure 4. Location of process control sensors (adapted from [10]).

directly observe the temperature profile along the main flow direction in the DCS. In addition, safety measures such as oxygen sensors are also available.

4.2 Distributed Temperature Measurement

Two different fiber-optic based temperature methods are applied at the test rig. Primarily, temperature measurement via Rayleigh effect is used. For this method, the backscattering, which results if light interacts with impurities in the fiber-optic, is measured (for details see [24–26]). The processing unit available is capable of handling one optical fiber up to a length of 20 m at a time. The test PFHEs are equipped with seven optical fibers each, summing up to a total fiber length of around 200 m (see Fig. 5).

Temperatures can be collected along the fibers at an interval of a few mm. The signal of the sensors is affected by temperature and strain of the fiber. To solely obtain the temperature signal, the fibers are fed through metal capillary tubes, where they can expand and contract without hindrance. Part of the capillary tubes are attached to the surface of the PFHE with aluminum tape, whereas other fibers run through the inside of the PFHE in blank layers, which are dedicated for this purpose (Fig. 6).

As a result, it is possible to measure temperatures at the surface, as well as within the PFHE. The fibers are arranged in such a way that temperature profiles in all spatial directions can be derived.

For the Rayleigh optical fibers, as well as some other measurement systems at
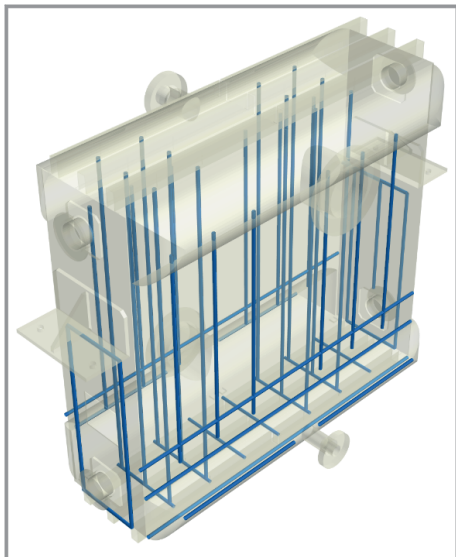
Figure 3. 3D model of the test rig (adapted from [3]).

Figure 5. Location of Rayleigh optical fibers.

the test rig, there is one important limitation. More sensors are installed at the test rig than can be evaluated at the referring processing unit at the same time. In fact, the warmup and cooldown cycles shall be repeatable in order to gain an overall view from the measurements of different sensors that were recorded successively at different cycles.

Another fiber-optical temperature measurement technology that is examined at the test rig is fiber Bragg grating (FBG). Unlike Rayleigh fibers, the temperature cannot be measured over the entire length of the fiber, only at particular positions of the fiber, which were modified accordingly. The gratings cause light reflection of a certain wavelength, while all other wavelengths are transmitted. A detailed description of the method can be found in [26–29]. FBGs bring certain benefits in application and evaluation compared to the Rayleigh measurements and are to be qualified as a measurement method for cryogenic applications in the test rig. Thus, four FBG optical fibers are installed at one of the PFHEs at the test rig, three on the inside and one at the

surface. The fibers run through the same capillary tubes as the Rayleigh fibers to enable simple comparison of the two measurement technologies. Each of the fibers contains 13 FBG sensors at a distance of a few centimeters.

4.3 Strain Measurement

In addition to temperature, strain can also be measured using Rayleigh optical fibers. To this end, the fibers are attached directly to the surface of the PFHE using aluminum tape to record the strain of the underlying metal (Fig. 6a). Since the fiber signal is also affected by the temperature, this temperature-induced effect is subtracted from the total signal [26] to solely obtain the strain signal. Therefore, the strain fibers run parallel to the temperature measurement fibers on the surface of the PFHE (see Fig. 5), which only collect the temperature signal that can be subtracted from the signal of the strain fiber at the respective location. Using Rayleigh fiber-optical measurement, it is possible to detect the spatially resolved total strain as well as integral deformation along the direction of the fiber.

As an additional strain measurement technology, strain gauges are installed at the PFHE test specimen (see [30] for information about strain gauges). Three strain gauges each are combined to a strain gauge rosette, by which the full 2D stress state can be obtained. The strain gauge rosettes are located at critical areas, where high temperature gradients are expected. In total, around 40 strain gauge rosettes are installed at the PFHE test specimen. The strain gauges are glued directly to the surface of the PFHE using a special adhesive. The strain gauge rosettes detect the total strain. The thermal expansion can be subtracted to ascertain just the mechanical strain of the underlying metal. For this reason, compensation strain gauges are installed. These sensors are glued to very small aluminum plates, which in turn are mounted on the surface of the PFHEs using a heat-conducting paste. Thus, the aluminum plates show the same temperature and thermal expansion as the underlying metal but are subject to negligible mechanical strain due to the small size of the plates. In the result section the strain equivalent ε_v is used to depict the measurement results. This von-Mises type stress equivalent is a scalar expression, that can be derived from the principal stresses ε_1 and ε_2 (Eq. (1)).

$$\varepsilon_v = \sqrt{\varepsilon_1^2 + \varepsilon_1^2 - \varepsilon_1 \varepsilon_2} \qquad (1)$$

4.4 Damage Detection

One of the main goals of the test rig is to detect the appearance of a fatigue damage. Two different damage symptoms are expected: cracks and leakages.
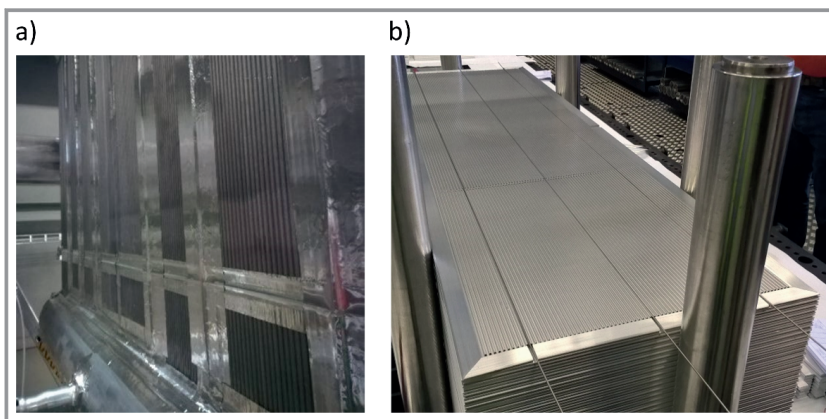

Figure 6. Attachment of optical fibers a) to the surface and b) inside the PFHE.

The appearance of cracks at the PFHE is detected by visual monitoring. Hence, critical areas of the PFHEs are equipped with webcams in a special camera housing, which create an empty space within the perlite insulation. Visual monitoring is completed by endoscope cameras that are mounted to monitor critical areas from another ankle.

In addition to cracks, another type of damage that may occur at the test rig is leakage. There are two different types of leakage: Leakage from the inside of the PFHE to the surroundings (external leakage), and leakage between two layers within the heat exchanger (internal leakage) [7, 12]. Leakage is detected using gas-based methods. Depending on the type of leakage, two different methods are applied.

To recognize external leakage, 5–10 vol % of helium (He) are added to the gaseous nitrogen, which serves as the process medium. Hence, helium flows through all active layers of the PFHEs and the piping of the test rig (see Fig. 7a). Since the test rig is operated at a pressure of approximately 5.5 bar, helium-containing gas will leak from the PFHEs in the event of severe damage. The dummy layers are also filled with helium at gauge pressure. Crucial parts of the PFHEs are constantly monitored to check for helium

leakage during operation. If leakage occurs, each PFHE module can be monitored separately to locate the leakage.

Internal leakage detection is more sophisticated. Internal leakage occurs between two active layers within the PFHE, in our case, by default, one cold and one warm layer. To detect such damages, the gas compartments on the cold and warm side of the PFHE are separated from the closed circular flow. The warm side is filled with a mixture of nitrogen and hydrogen (approx. 5 vol % H_2) at a gauge pressure of around 5 bar. The cold side is evacuated using two vacuum pumps (see Fig. 7b). In the event of internal leakage, hydrogen enters the cold side from a warm layer and is detected by a leakage detector. The leakage can be assigned to one of the PFHEs, since they can be separated from the leakage detector individually. Hydrogen is used here because the cold side is contaminated with helium due to the external leakage detection. Internal leakage cannot be detected during test rig operation, owing to the application of the vacuum pumps and separation of the gas compartments. Hence, testing for internal leakage is conducted regularly during test rig downtime.

5 Results and Discussion

In this chapter, some exemplary results of different measurement systems are presented to show the capabilities of the applied measurement systems. In Fig. 8 the temperature T measured by three Pt100 temperature sensors at the surface of one PFHE is shown for one cycle. In the first half of the cycle, the PFHE is cooled down and temperatures are dropping. In the second half, the PFHE is warmed up again and temperatures rise. All three temperature sensors show the same trend. Nevertheless, they experience different temperature drops depending on their distance to the cold end of the heat exchanger. Hence, the expected temperature profile from cold gas inlet to warm gas inlet prevails within the PFHE. The warm end of the PFHEs is kept at a temperature of around 50 °C throughout the cycle.

The graph in Fig. 9 shows the strain equivalent ε_v of one exemplary strain gauge rosette over one cycle. In accordance with foregoing modeling [10], two peaks in strain are observed, both shortly after the gas feed is changed from warm to cold and vice versa. This is due to the highest temperature gradient at the beginning of the respective gas supply.

Finally, fiber-optical temperature measurements obtained from the Rayleigh sensors are presented. Fig. 10 shows the results of one fiber section at different times in the cooldown phase of one cycle. At the beginning, a temperature of around 45 °C prevails throughout almost the entire PFHE length. Afterwards, the PFHE is continuously cooled down from the cold end until a minimum temperature of approx. −110 °C is reached at the end of the cooldown phase (relative cycle time: 0.50) for this particular fiber section. The local minimum in the temperature profiles is due to the
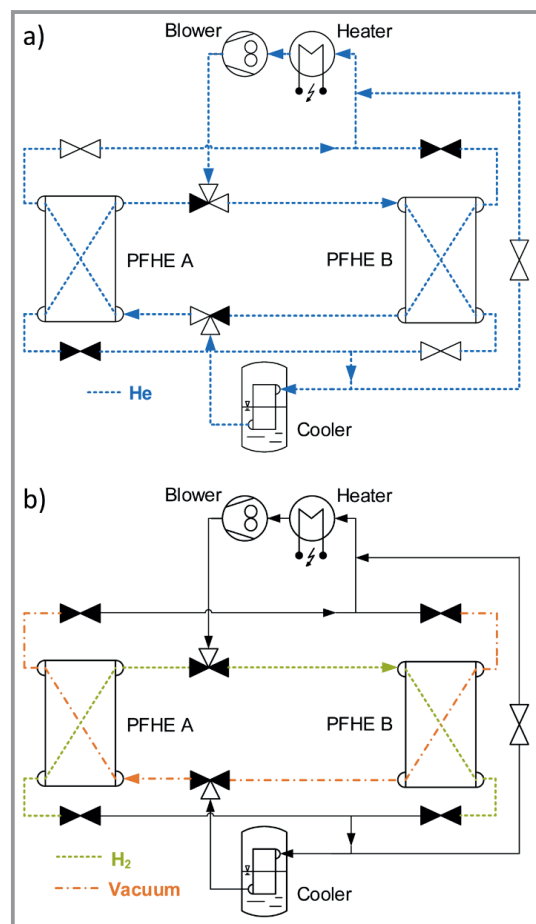
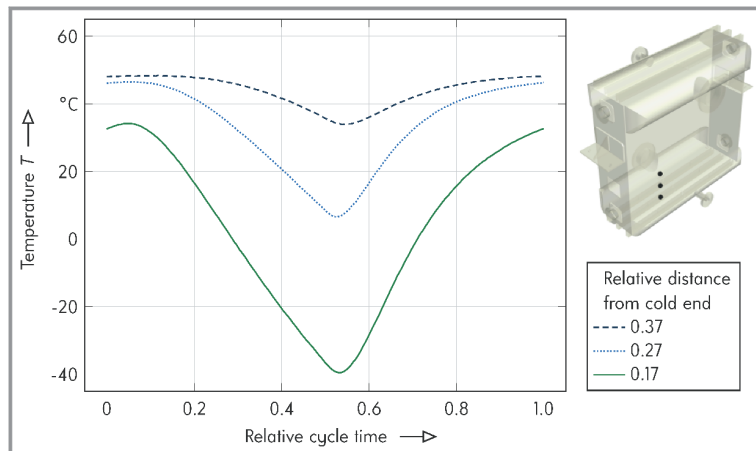**Figure 7.** Detection of a) external and b) internal leakage.

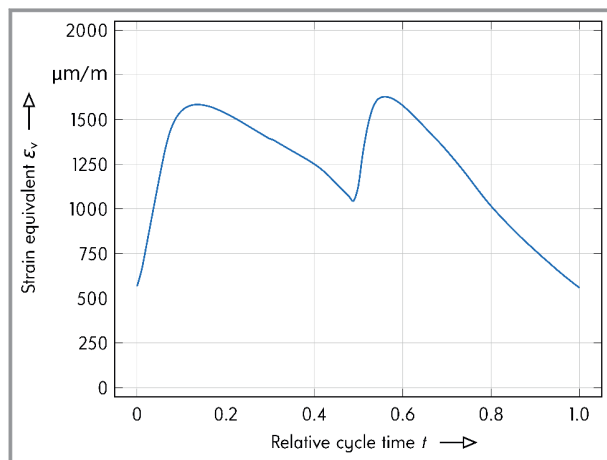**Figure 8.** PFHE surface temperatures of one cycle.

Figure 9. Cyclic strain measured by strain gauge.

different heat transfer coefficients along the gas pathway through the PFHE. The fins, which are provided to increase heat transfer, show higher heat transfer coefficients than the distributor fins. Hence, cooling is faster where the cold gas enters the area with this type of fins (see Fig. 1b). Fig. 10 shows that dynamic, distributed temperature measurements are possible using Rayleigh optical fibers.

While the presented results were for just one cycle, over 1000 cycles per PFHE have been carried out at the test rig. Results from different cycles were compared to each other and showed good agreement in terms of temperature and strain.

6 Conclusion

A large test rig to investigate fatigue effects in the main heat exchangers of flexible air separa-

tion units has been designed, constructed, and successfully put into operation. The test rig is operated at realistic temperature and pressure levels using gaseous nitrogen as a process medium. It contains two PFHEs, which are larger than those in previous experiments and designed to capture all effects of dynamic operation and exhibit realistic behavior. The PFHEs undergo a highly periodic series of cooldowns and warm-ups as a test scenario, which is intended to provoke fatigue damage after a reasonable amount of time.

The test rig is extensively equipped with measurement technology not only for process control, but also to collect 3D temperature and strain data, as well for detection of provoked fatigue damages. All measurement systems provided are in good working order, and some exemplary results have been presented in this paper.

The operation of this test rig will provide thorough insights into the behavior of plate-fin heat exchangers under highly dynamic operation and help to validate and improve computational lifetime investigation tools, which in turn can predict the mechanical stress on PFHEs in a flexible ASU or other relevant industrial processes. The results from the test rig may significantly affect the way PFHEs are designed and operated in processes where dynamic operation is necessary.
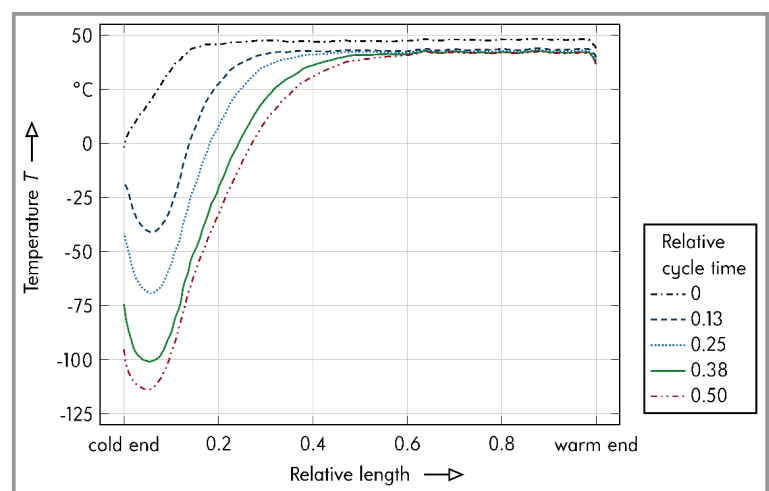
Figure 10. Cooldown measured by one Rayleigh optical fiber section.

Symbols used

| T | [°C] | Temperature |

Greek letters

| $\varepsilon_{1,2}$ | [μm m^{-1}] | Principle strains |
| ε_{v} | [μm m^{-1}] | Strain equivalent |

Abbreviations

ASU	Air separation unit
BiK	Block-in-Kettle
DCS	Distributed control system
FBG	Fiber Bragg grating
LIN	Liquid nitrogen
PFD	Process flow diagram
PFHE	Plate-fin heat exchanger

References

[1] www.kopernikus-projekte.de/start (Accessed on November 06, 2020)

[2] A. Sauer, E. Abele, H. U. Buhl, *Energieflexibilität in der deutschen Industrie: Ergebnisse aus dem Kopernikus-Projekt – Synchronisierte und energieadaptive Produktionstechnik zur flexiblen Ausrichtung von Industrieprozessen auf eine fluktuierende Energieversorgung (SynErgie)*, Fraunhofer Verlag, Stuttgart **2019**.

[3] H. Klein, P. Fritsch, P. Haider, R. Kender, F. Rößler, S. Rehfeldt, P. Freko, R. Hoffmann, I. Thomas, B. Wunderlich, *Chem. Ing. Tech.* **2020**, *92 (12)*, 1921–1940. DOI: https://doi.org/10.1002/cite.202000054

[4] R. Kender, B. Wunderlich, I. Thomas, A. Peschel, S. Rehfeldt, H. Klein, *Chem. Eng. Res. Des.* **2019**, *147*, 98–112. DOI: https://doi.org/10.1016/j.cherd.2019.04.031

[5] A. Obermeier, C. Windmeier, E. Esche, J.-U. Repke, *Chem. Eng. Sci.* **2019**, *195*, 904–920. DOI: https://doi.org/10.1016/j.ces.2018.10.036

[6] P. Freko, I. Thomas, R. Hoelzl, A. Lehmacher, A. Woitalka, in *International Heat Transfer Conference 15*, **2014**, 3715–3725. DOI: https://doi.org/10.1615/IHTC15.hex.009791

[7] P. Carter, T. J. Carter, A. Viljoen, *Eng. Failure Anal.* **1996**, *3 (1)*, 29–43. DOI: https://doi.org/10.1016/1350-6307(95)00031-3

[8] R. Hölzl, in *Proc. of the ASME 2012 Pressure Vessels & Piping Conference* **2012**, 871–875. DOI: https://doi.org/10.1115/PVP2012-78343

[9] A. Woitalka, I. Thomas, P. Freko, A. Lehmacher, in *Proc. of International Symposium on Advances in Computational Heat Transfer* **2015**, 11. DOI: https://doi.org/10.1615/ICHMT.2015.IntSympAdvComputHeatTransf.10

[10] P. Haider, P. Freko, S. Lochner, T. Reiter, S. Rehfeldt, H. Klein, *Chem. Eng. Res. Des.* **2019**, *147*, 90–97. DOI: https://doi.org/10.1016/j.cherd.2019.04.025

[11] P. Haider, P. Freko, T. Acher, S. Rehfeldt, H. Klein, *Appl. Therm. Eng.* **2020**, *180*, 115791. DOI: https://doi.org/10.1016/j.applthermaleng.2020.115791

[12] R. Hölzl, R. Flüggen, in *Proc. of the ASME 2013 Pressure Vessels and Piping Conference* **2013**, V003T03A093. DOI: https://doi.org/10.1115/PVP2013-97915

[13] R. Hölzl, T. Hecht, P. Freko, in *Proc. of the ASME Pressure Vessels & Piping Division Conference* **2014**, V003T03A045. DOI: https://doi.org/10.1115/PVP2014-28391

[14] R. Niroomand, M. H. Saidi, S. K. Hannani, *Appl. Therm. Eng.* **2019**, *157 (1)*, 113730. DOI: https://doi.org/10.1016/j.applthermaleng.2019.113730

[15] E. Buyruk, K. Karabulut, *Heat Transfer Eng.* **2018**, *39 (15)*, 1392–1404.

[16] E. Buyruk, K. Karabulut, Ö. O. Karabulut, *Heat Mass Transfer* **2013**, *49 (6)*, 817–826. DOI: https://doi.org/10.1007/s00231-013-1129-8

[17] *Industrial Gases Processing* (Ed: H.-W. Häring), Wiley-VCH, Weinheim **2008**.

[18] H. Hausen, H. Linde, *Tieftemperaturtechnik: Erzeugung sehr tiefer Temperaturen, Gasverflüssigung und Zerlegung von Gasgemischen*, Springer, Berlin **1985**.

[19] J. Stichlmair, H. Klein, S. Rehfeldt, *Distillation: Principles and practice*, Wiley-AIChE, Wiley, Hoboken, NJ **2021**.

[20] J. E. Hesselgreaves, R. Law, D. A. Reay, in *Compact heat exchangers: Selection, design and operation* (Eds: J. E. Hesselgreaves, R. Law, D. A. Reay, P. J. Heggs), Butterworth-Heinemann, Oxford **2017**.

[21] www.linde-engineering.com/en/about-linde-engineering/success-stories/managing-heat-efficiently (Accessed on November 06, 2020)

[22] R. K. Shah, A. C. Mueller, D. P. Sekulic, in *Ullmann's Encyclopedia of Industrial Chemistry*, Vol. 82, Wiley-VCH Verlag, Weinheim **2000**.

[23] *Handbook of heat transfer* (Eds: W. M. Rohsenow, J. P. Hartnett, Y. I. Cho), 3rd ed., McGraw-Hill, New York **1998**.

[24] www.rp-photonics.com/rayleigh_scattering.html (Accessed on November 06, 2020)

[25] A. Al-Azzawi, *Fiber Optics: Principles and Practices*, Taylor and Francis, Hoboken **2006**.

[26] H.-E. Joe, H. Yun, S.-H. Jo, M. B. G. Jun, B.-K. Min, *Int. J. Precis. Eng. Manuf. – Green Tech.* **2018**, *5 (1)*, 173–191. DOI: https://doi.org/10.1007/s40684-018-0017-6

[27] V. G. Schlüter, *Entwicklung eines experimentell gestützten Bewertungsverfahrens zur Optimierung und Charakterisierung der Dehnungsübertragung oberflächenapplizierter Faser-Bragg-Gitter-Sensoren*, BAM-Dissertationsreihe, Vol. 56, Bundesanstalt für Materialforschung und -prüfung (BAM), Berlin **2010**.

[28] M. Schmid, M. Müller, A. Koch, in *Proceedings SENSOR 2015*, **2015**, 545–549. DOI: https://doi.org/10.5162/SENSOR2015/D3.1

[29] K. O. Hill, Y. Fujii, D. C. Johnson, B. S. Kawasaki, *Appl. Phys. Lett.* **1978**, *32 (10)*, 647–649.

[30] www.me-systeme.de/produkte/dehnungsmessstreifen/tech-notes/TN-515-Rosetten_de.pdf (Accessed on November 06, 2020)